CHEMISTRY OF MATERIALS

ARTICLE

pubs.acs.org/cm

Solvothermal Synthesis and Characterization of Large-Crystal All-Silica, Aluminum-, and Boron-Containing Ferrierite Zeolites

V. R. Reddy Marthala,[†] Michael Hunger,[†] Florian Kettner,[‡] Harald Krautscheid,[‡] Christian Chmelik,[§] Jörg Kärger,[§] and Jens Weitkamp[†,*]

[†]Institute of Chemical Technology, University of Stuttgart, 70550 Stuttgart, Germany

[‡]Institute of Inorganic Chemistry and [§]Department of Interface Physics, University of Leipzig, 04103 Leipzig, Germany

ABSTRACT: Large crystals of all-silica, aluminum-, and boron-containing ferrierite zeolites were synthesized using a solvothermal synthesis method and a fluoride medium. Alkylamines, namely, propylamine, butylamine, and pentylamine were employed as templates in the syntheses. The products were characterized by powder X-ray diffraction (XRD), inductively coupled plasma-optical emission spectrometry (ICP-OES), thermogravimetric analysis (TGA), elemental (CHN) analyses, scanning electron microscopy (SEM), N_2-adsorption, and ^{1}H, ^{11}B, ^{27}Al, as well as ^{29}Si MAS NMR spectroscopy. The ^{27}Al and ^{11}B MAS NMR spectroscopic investigations revealed that aluminum and boron were successfully incorporated into the FER-type framework. SEM indicated the occurrence of crystals with a size of up to about 600 μm. Furthermore, for all-silica and boron-containing ferrierite zeolites, the shape, size, and thickness of the crystals could be controlled by increasing the chain length of the alkyl group in the alkylamine and the crystallization time. Aluminum-containing ferrierite zeolites could be synthesized with a rectangular morphology exclusively. Observation of transient guest profiles during methanol uptake by means of IR microscopy exemplifies the possibility of directly observing diffusion anisotropy in FER-type frameworks.

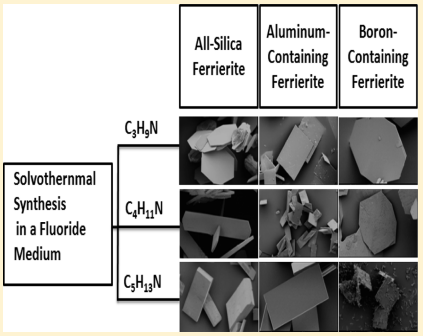

KEYWORDS: large zeolite crystals, ferrierite, boron-containing zeolites, IR microscopy

1. INTRODUCTION

Since the first successful preparation of synthetic zeolites in 1948,[1] these microporous materials have been applied on an industrial scale in heterogeneous catalysis, adsorptive separation, and ion exchange. Research on zeolite synthesis is mainly focused on routes for the preparation of either large crystals or nanocrystals. Although nanocrystalline zeolites with high surface area are advantageous in heterogeneous catalysis, large-crystal zeolites are preferred for some specific purposes. Particularly, large-crystal zeolites are essential in the precise crystal structure determination,[2] the preparation of nanodevices,[3] shape-selective catalysis,[4] and the study of the adsorption and diffusion of guest molecules.[5,6]

The synthesis of large-crystal zeolites has been achieved by employing different methods,[7−10] such as modified hydrothermal synthesis methods (e.g., fluoride route and bulk material dissolution), low-temperature gel methods, and nonaqueous solvothermal synthesis methods (e.g., using nonaqueous solvents in fluoride medium). Often, large-crystal siliceous MFI- (e.g., silicalite-1) and FAU-type (e.g., zeolites X and Y) zeolites have been synthesized using modified hydrothermal syntheses and low-temperature gel methods,[7,8] while the nonaqueous solvothermal synthesis method is particularly utilized to prepare large crystals of zeolite ferrierite.[9−12]

Zeolite ferrierite contains a two-dimensional channel system with a straight 10-membered ring pore system (0.42 × 0.54 nm) along the [0 0 1] direction, which is interconnected by an 8-membered-ring pore system (0.35 × 0.48 nm) along the [0 1 0] direction.[13] Though the natural ferrierite mineral has been discovered by Graham as early as 1918,[14] the synthesis of ferrierite zeolites was successful only in the 1960s.[15,16] These zeolites have been prepared using different templates and synthesis methods.[9,12,17−22] Ozin and co-workers[9,11] were the first to synthesize large-crystal siliceous and aluminum-containing ferrierite zeolites using the nonaqueous solvothermal synthesis method under fluoride medium. In contrast to the hydrothermal synthesis method, the solvothermal synthesis method uses viscous solvents and mineralizing agents. In addition, a small amount of water is used as reactant. The use of solvents with intermediate viscosity, such as pyridine rather than water in the synthesis, reduces the chances of secondary nucleation and prevents the formation of small crystals.[10] In addition, during the crystallization period, mass transfer in the synthesis gel occurs by diffusion rather than convection. Hence, the solvothermal synthesis method leads to the formation of large-crystal zeolites.[10]

On the other hand, Wirnsberger et al.[22] synthesized large-crystal all-silica ferrierite zeolites using the solvothermal method reported by Kuperman et al.,[9] but with different *n*-alkylamines as templates. These authors reported that by using different *n*-alkylamines, namely, *n*-propylamine, *n*-butylamine, and *n*-pentylamine as templates and pyridine as solvent, the crystal morphology of the

Received: May 27, 2010
Revised: March 9, 2011
Published: April 27, 2011

Table 1. Survey of the Zeolite Samples Studied, Details of the Synthesis Parameters, and Crystal Morphologies of the Products[a]

batch	template	t^b/ days	T^c/ K	n_{Si}/n_{Al}[e] or n_{Si}/n_B[f] gel	n_{Si}/n_{Al}[e] or n_{Si}/n_B[f] product	crystal phase	crystal shape	crystal size[d]/μm
A1	propylamine	12	453	NA[g]	ND[h]	FER	hexagonal	ca.600
A2	butylamine	20	453	NA[g]	1200	FER	stretched hexagonal	ca.400
A3	pentylamine	45	433	NA[g]	5320	FER	thick rectangular flat	ca.300
B1	propylamine	12	453	6	14	FER	rectangular flat	ca.100
B2	butylamine	20	453	6	16	FER	rectangular flat	ca.150
B3	pentylamine	45	453	6	17	FER	rectangular flat	ca.180
C1	propylamine	12	453	3	35	FER	stretched hexagonal/octagonal with rough surfaces	ca.150
C2	butylamine	20	453	3	65	FER	octagonal	ca.50
C3	pentylamine	45	453	3	50	FER+MFI	combination of small stretched hexagonal and large squares	ca.100
C4	propylamine	12	453	6	100	FER	octagonal	ca.150
C5	butylamine	20	453	6	150	FER	octagonal	ca.50
C6	pentylamine	45	453	6	325	FER	rectangular flat	ca.100

[a] Batches A1 to A3 represent all-silica ferrierites, batches B1 to B3 represent aluminum-containing ferrierites, and batches C1 to C6 represent boron-containing ferrierites. [b] Crystallization time. [c] Crystallization temperature. [d] Of the largest faces along the [0 0 1] direction. [e] Batches A1 to A3 and B1 to B3. [f] Batches C1 to C6. [g] Not applicable (i.e., no aluminum source was added to the gel). [h] Not detected by ICP-OES.

products can be controlled. Similarly, in our previous work, by modifying the synthesis method of Kuperman et al.[9] and by using different *n*-alkylamines as templates and pyridine as solvent, large-crystal all-silica ferrierite zeolites with different morphologies have been synthesized.[12]

Though several references are available on the incorporation of aluminum,[23] gallium,[24] iron,[25] titanium,[26] and vanadium[27] into the framework of regularly sized, pure ferrierite crystals, the literature concerning the isomorphous substitution of silicon by heteroatoms, such as aluminum or boron, into the framework of large-crystal ferrierite zeolites is very scarce. Up to now, most studies of large-crystal ferrierite zeolites were aiming at the synthesis and characterization of all-silica ferrierite zeolites[9,11,12,22] and a few at large-crystal aluminum-containing ferrierite zeolites.[9,11,28,29] Moreover, to the best of our knowledge, the synthesis of large-crystal boron-containing ferrierite zeolites has not been reported at all. Though Gies and his group[17,18] attempted to synthesize boron-containing ferrierite zeolites, their endeavors were unsuccessful. In addition, their synthesis method yielded a product with mixed FER and MFI phases (FER and MFI are the three-letter codes of the International Zeolite Association for zeolites with the ferrierite and ZSM-5 frameworks, respectively). Here, we report on a systematic study devoted to the solvothermal synthesis of large-crystal all-silica, aluminum-containing, and boron-containing ferrierite zeolites using different alkylamines as templates. In addition, we evidenced the successful incorporation of aluminum and boron into the large-crystal FER-type framework by solid-state NMR spectroscopy.

Framework stability during sample activation made all-silica ferrierite an ideal model system for systematic diffusion studies by exploiting the options of microimaging via interference microscopy (IFM) and IR microscopy (IRM) for monitoring transient concentration profiles during guest uptake and release.[5,6,12] In these studies it turned out that molecular uptake and release mainly occurred through the 8-membered-ring channels rather than the 10-membered-ring channels. This rather peculiar behavior can be attributed to a blockage of the entrances of the 10-membered-ring channels[5,6] and prohibits the exploitation of a feature which makes FER-type frameworks particularly attractive for diffusion studies, namely, the direct observation of diffusion anisotropy. Hence, simultaneously with extending the range of possible compositions, it was also one goal of the present study to obtain FER-type zeolite crystals in which both channel systems are accessible from the external surface.

2. EXPERIMENTAL SECTION

2.1. Synthesis of All-Silica Ferrierite Zeolites. The synthesis of all-silica ferrierite zeolites was carried out according to the procedure published previously.[12] A typical synthesis procedure was as follows: Initially, pyridine (≥99%, Fluka) and an alkylamine, namely, propylamine (98%, Janssen Chemica), butylamine (≥99%, Merck), or pentylamine (≥98%, Merck), were mixed quantitatively in a polypropylene beaker. To this mixture, concentrated hydrofluoric acid (40%, Sigma-Aldrich) was carefully added in a dropwise manner. Then, the mixture was vigorously stirred for 1 h at room temperature. Subsequently, fumed silica (Cab-osil M5, Cabot) was slowly added in portions, and an opaque gel with low viscosity was obtained. Finally, water was added to obtain a clear solution. This solution was stirred for another 1 h at room temperature and transferred into a 300 mL stainless steel autoclave containing an inner PTFE cylinder. The molar composition of a typical synthesis batch was $1.5SiO_2$:$8.0H_2O$:$2.0HF$:$4.0C_nH_{2n+1}NH_2$ (where, n = 3 to 5):$16.0C_5H_5N$. The crystallization times and temperatures are given in Table 1. At the end of the crystallization period, the product was recovered by filtration, washed with methanol, several times with demineralized water, and finally again with methanol.

2.2. Synthesis of Aluminum- and Boron-Containing Ferrierite Zeolites. Incorporation of aluminum or boron into the framework of ferrierite zeolite during the synthesis was achieved by the following procedure: As described in Section 2.1, after preparation of the synthesis mixture consisting of pyridine, the alkylamine, hydrofluoric acid, fumed silica, and water, either the aluminum source, namely, Pural SB (74% Al_2O_3, Sasol) or the boron source, namely, boric acid (>99.5%, Fluka), and organic cations, namely, tetrapropylammonium bromide (TPABr), were slowly added. Since no alkali was used in the present synthesis method, tetrapropylammonium (TPA^+) ions act as organic cations to compensate the negative charge of the zeolite framework generated by the incorporation of aluminum or boron. Subsequently, this mixture was stirred for 1 h at room temperature. Afterward, the clear solution was transferred into a 300 mL stainless steel autoclave containing a PTFE insert. The molar gel composition of the aluminum- and boron-containing gels were $1.5SiO_2$:$0.125Al_2O_3$:$8.0H_2O$:$2.0HF$:4.

$0C_nH_{2n+1}NH_2$ (where, n = 3 to 5):16.0C_5H_5N and 1.5SiO_2:(0.125−0.25)B_2O_3:8.0H_2O:2.0HF:4.0$C_nH_{2n+1}NH_2$ (where, n = 3 to 5):16.0C_5H_5N, respectively. The crystallization times and temperatures are given in Table 1. The products were recovered as described in Section 2.1.

2.3. Postsynthesis Treatments. To obtain a clean surface of the large ferrierite crystals, about 1 g of the as-synthesized material was kept in contact with 0.1 M NaOH (100 mL) solution for 2 days at room temperature. Subsequently, these samples were collected by filtration, washed with 500 mL of demineralized water, dried at 353 K, and calcined under a flow of synthetic air. The calcination of all-silica ferrierite zeolites was carried out at 1123 K for 3 days, while the calcination of the aluminum- and boron-containing ferrierite zeolites was performed at 873 K for 4 days. In contrast to all-silica ferrierite zeolites, aluminum- and boron-containing ferrierite zeolites are not stable at higher calcination temperatures (i.e., at 1123 K). Therefore, these ferrierite zeolites were calcined at 873 K.

2.4. Characterization. Powder X-ray diffractograms were collected on a Bruker D8 instrument with Cu−Kα radiation (λ = 0.514 nm). The X-ray diffraction (XRD) patterns were recorded in the range of 2θ = 5 to 50°. The chemical analysis by inductively coupled plasma-optical emission spectrometry (ICP-OES) of the products was performed using a Varian Vista-MPX spectrometer. Prior to the analysis, the solid materials were dissolved in a mixture of concentrated acids, namely, HF (3 mL), HCl (2 mL), and HNO_3 (2 mL). Thermogravimetric analysis (TGA) was carried out on a Setsys 16/18 (Setaram) instrument in the temperature range of 303 to 973 K in a flow of synthetic air, while the elemental (CHN) analysis was carried out on a Vario EL cube analyzer. The morphological studies were carried out on a Cambridge CAM SCAN 44 electron microscope. Since the solid sample must be electrically conductive for the scanning electron microscopy (SEM) measurements, gold sputtering was done prior to the studies. N_2-adsorption measurements were performed using a Quantachrome Autosorb instrument. Before N_2-adsorption, the calcined samples were activated at a pressure of $p < 10^{-2}$ mbar for 15 h at 623 K.

2.5. Solid-State NMR Measurements. The solid-state NMR spectroscopic investigations were performed on a Bruker AvanceIII 400 WB spectrometer. ^{29}Si MAS NMR spectra were recorded at a resonance frequency of 79.5 MHz using a 7 mm MAS NMR probe with a sample spinning rate of about 3.5 kHz. The spectra were obtained by applying the dipolar decoupling technique (HPDEC). A pulse length of 5 μs and a recycle delay of 10 s were applied. ^{1}H, ^{11}B, and ^{27}Al MAS NMR spectra were acquired at resonance frequencies of 400.0, 128.3, and 104.2 MHz, respectively, using a 4 mm MAS NMR probe with a sample spinning rate of about 9.0 kHz. Prior to all ^{1}H and the ^{11}B MAS NMR measurements with sample C5 on the calcined materials, the samples were dehydrated at 723 K under vacuum ($p < 10^{-2}$ mbar) using a vacuum line. ^{1}H, ^{11}B, and ^{27}Al MAS NMR spectra were recorded by applying single pulse excitation with pulse lengths of 4.0, 1.0, and 0.61 μs and repetition times of 10, 2, and 0.5 s, respectively. In the case of most of the ^{11}B and all ^{27}Al MAS NMR spectroscopy measurements, the samples were fully hydrated over a saturated aqueous solution of $Ca(NO_3)_2$ for at least 12 h. For the samples hydrated in a desiccator, the ^{11}B and the ^{27}Al MAS NMR spectra were recorded immediately after collecting the samples from the desiccator.

3. RESULTS AND DISCUSSION

In Table 1, the synthesis batches including the templates employed, the crystallization time, the crystallization temperature, the n_{Si}/n_{Al} or n_{Si}/n_B ratios of the synthesis gel and of the as-synthesized products, the crystal shapes and sizes of the series of large-crystal all-silica, aluminum-containing, and boron-containing ferrierite zeolites are given. The synthesis batches from A1 to A3, B1 to B3, and C1 to C6 correspond to all-silica, aluminum-containing, and boron-containing ferrierite zeolites, respectively. Alkylamines, namely, propylamine, butylamine, and pentylamine, were used as templates in the syntheses. As reported previously,[12,22] the crystallization time increases with increasing length of the alkyl group in the amine. Therefore, crystallization times of 12, 20, and 45 days were used when the synthesis was performed with propylamine (batches A1, B1, C1, and C4), butylamine (batches, A2, B2, C2, and C5), and pentylamine (batches A3, B3, C3, and C6) as templates, respectively. Except for sample A3, all samples were crystallized at 453 K. For sample A3, a crystallization temperature of 433 K was chosen as reported in our previous publication.[12]

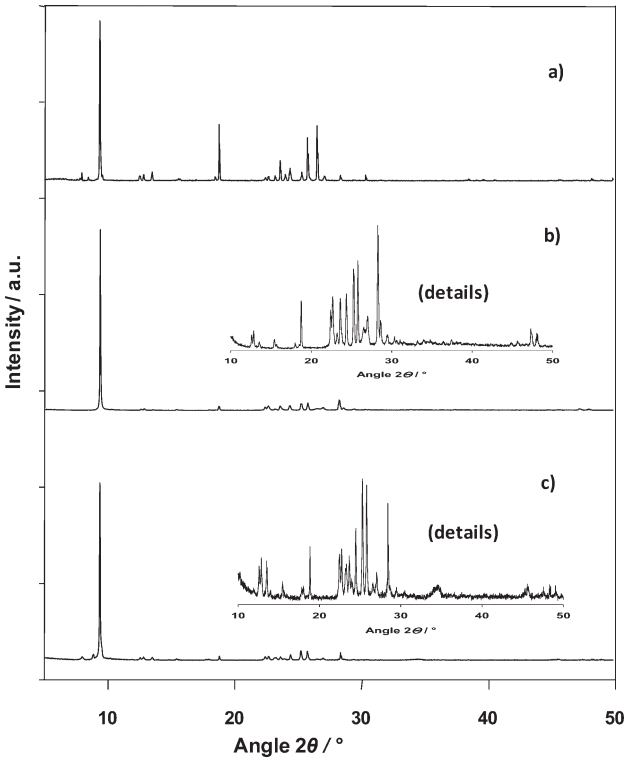

Figure 1. XRD patterns of as-synthesized all-silica (a), sample A3, aluminum-containing (b), sample B3, and boron-containing (c), sample C6, ferrierite zeolites synthesized using pentylamine as template.

The powder XRD patterns of all products except sample C3 show reflections which are typical for the FER structure. For sample C3, a mixture of FER and MFI phases was found. As examples, the XRD patterns of the all-silica (batch A3), aluminum-containing (batch B3), and boron-containing (batch C6) ferrierite samples synthesized using pentylamine as template are depicted in Figure 1. The patterns show the typical reflection line of the (0 0 2) plane at about 2θ = 9.5° with an extremely large intensity in comparison with the lines of the other planes. This is due to the nonisotropic orientation of the crystals with a distinct orthorhombic flat prismatic morphology in the powder samples consisting of large-crystal ferrierite zeolites.

To find out whether or not the calcination procedure carried out at 873 K for aluminum- and boron-containing ferrierite zeolites was successful, thermogravimetric (TG) and elemental (CHN) analyses, as well as ^{1}H MAS NMR spectroscopy, were performed. TGA of the calcined and hydrated sample (e.g., sample B3) in the temperature range of 303 to 973 K shows a

dx.doi.org/10.1021/cm1014898 |Chem. Mater. 2011, 23, 2521–2528

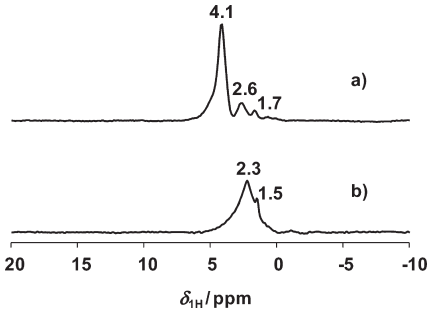

Figure 2. ^{1}H MAS NMR spectra of calcined aluminum-containing (a), sample B3, and boron-containing (b), sample C5, ferrierite zeolites.

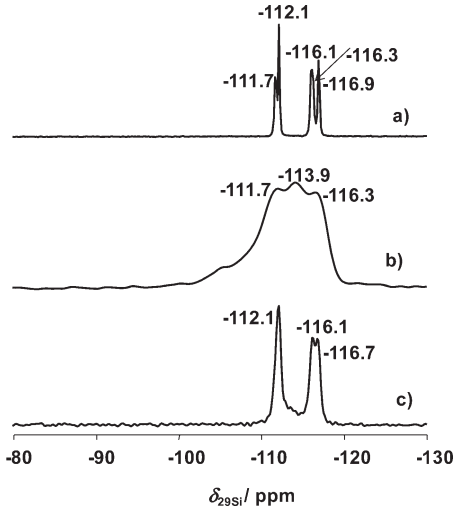

Figure 3. ^{29}Si MAS NMR spectra of calcined all-silica (a), sample A3, aluminum-containing (b), sample B3, and boron-containing (c), sample C6, ferrierite zeolites.

weight loss of about 6% between 303 and 473 K, while no weight loss was observed between 473 and 973 K. The weight loss between 303 and 473 K was due to the presence of physisorbed water in the sample. The CHN analysis of the calcined ferrierite sample (e.g., for sample B3) indicates the presence of only about 1% of carbon in comparison with the as-synthesized ferrierite samples. In addition, the ^{1}H MAS NMR spectra of the calcined aluminum-containing (Figure 2a) and boron-containing (Figure 2b) ferrierite zeolites did not show signals originating from the amine (i.e., template or solvent) species. The above-mentioned findings from TGA, CHN, and ^{1}H MAS NMR spectroscopic methods reveal that the calcination procedure described in Section 2.3 had brought about a complete removal of the template. The ^{1}H MAS NMR spectrum of the aluminum-containing ferrierite zeolite shows two weak signals at 1.7 ppm and 2.6 ppm due to SiOH groups and hydrogen-bonded AlOH groups, respectively. In addition, a strong signal at 4.1 ppm due to bridging hydroxyl groups was observed. The ^{1}H MAS NMR spectrum of the boron-containing ferrierite zeolite shows two peaks at 1.5 ppm and 2.3 ppm due to defect silanol groups and silanol groups in the vicinity of framework boron atoms (i.e., SiOH[B]), respectively. N_2-adsorption measurements were performed to find out whether or not the pore system of the calcined FER samples was accessible. The total pore volumes obtained at a relative pressure of 0.9 for samples

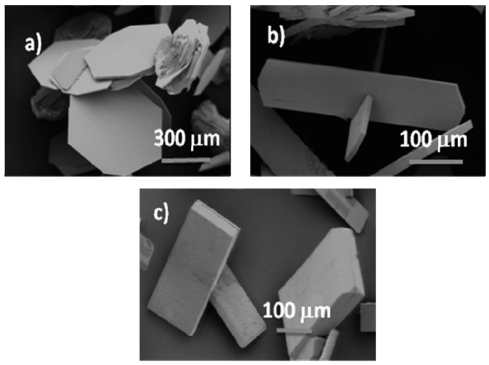

Figure 4. SEM images of the large-crystal all-silica ferrierite zeolites synthesized using propylamine (a) sample A1, butylamine (b), sample A2, and pentylamine (c), sample A3 as templates.

A3, B3, and C5 were 0.26 $cm^3\ g^{-1}$, 0.15 $cm^3\ g^{-1}$, and 0.20 $cm^3\ g^{-1}$, respectively. This finding shows that calcination was successful and the pore system of the ferrierite samples was accessible.[12]

Figure 3 represents the ^{29}Si MAS NMR spectra of a calcined all-silica, an aluminum-containing, and a boron-containing ferrierite. The ^{29}Si MAS NMR spectrum of the all-silica ferrierite (Figure 3a) exhibits an improved resolution and shows five peaks corresponding to five crystallographically nonequivalent Si sites in the asymmetric unit of space group *Pmnn*.[2,30,31] The signals at −116.3, −112.1, −116.1, −111.7, and −116.9 ppm are due to Si(1), Si(2), Si(3), Si(4), and Si(5) sites, respectively.[30,31] By contrast, the spectra of the aluminum-containing and the boron-containing ferrierites (Figures 3b and 3c) exhibit a considerably lower resolution and broader signals. This is due to the disorder of the local structure around silicon sites in the vicinity of aluminum or boron atoms incorporated into the framework of the zeolites.[28]

No aluminum source was added to the synthesis batches of the all-silica ferrierite samples (see Table 1, batches A1 to A3). Nevertheless, trace amounts of aluminum were detected by ICP-OES in the products of batches A2 and A3, which are probably due to the presence of impurities in the starting reagents. The SEM images of the large-crystal all-silica ferrierite zeolites are given in Figure 4. The morphology of the crystals obtained in the present work was similar to those of the samples synthesized in previous studies.[12,22] As evidenced by the SEM images in Figure 4, the morphology of the large-crystal all-silica ferrierite zeolites was controlled by the alkylamines used as templates and pyridine as solvent: When using propylamine as template and pyridine as solvent in the synthesis (batch A1), very large crystals (ca. 600 μm) of hexagonal morphology were obtained (Figure 4a). In agreement with previous reports,[12,22] upon increasing the chain length of the alkyl group in the template, that is, by using butylamine or pentylamine, large crystals with stretched hexagonal (ca. 400 μm, batch A2) and rather thick rectangular morphologies (ca. 300 μm, batch A3), respectively, were obtained (Figures 4b and 4c, respectively).

Ozin and co-workers[9,11] reported on the synthesis of large-crystal aluminum-containing ferrierite zeolites using the triethylamine trihydrofluoride complex as template and triethylamine or pyridine as solvents. Similar to our previous synthesis study,[12] we prepared in the present work large-crystal aluminum-containing ferrierite zeolites by modifying the synthesis method of Kuperman et al.[9] Alternatively, we used hydrogen fluoride and

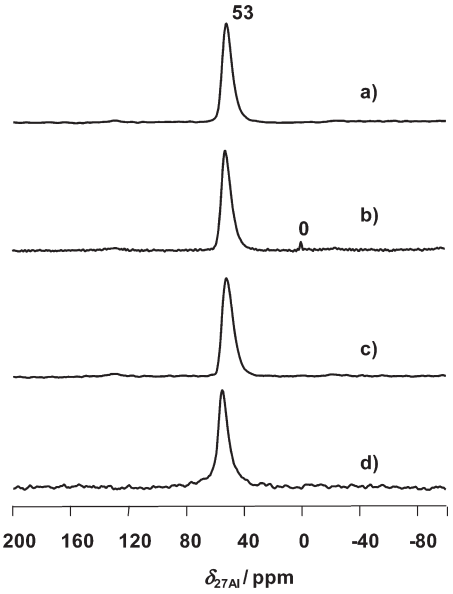

Figure 5. ^{27}Al MAS NMR spectra of as-synthesized large-crystal aluminum-containing ferrierite zeolites prepared using propylamine (a), sample B1, butylamine (b), sample B2, and pentylamine (c), sample B3, as templates. In (d), the spectrum of the calcined and rehydrated sample of (c) is shown.

alkylamines, namely, propylamine, butylamine, and pentylamine as templates and pyridine as solvent (see Section 2.2). As reported previously,[9,11] the n_{Si}/n_{Al} ratio of 6 was used in the synthesis gel (see Table 1). As a result, however, products with n_{Si}/n_{Al} ratios in the range of 14 to 17 (batches B1 to B3) were obtained. This is in good agreement with previous reports where the n_{Si}/n_{Al} ratio was 17.[9,11,28] In addition, we attempted to synthesize aluminum-containing ferrierite zeolites with n_{Si}/n_{Al} = 3 to 4.5 using propylamine as template (not mentioned in Table 1). Although the synthesis of aluminum-containing ferrierite zeolite with n_{Si}/n_{Al} = 4.5 in the synthesis gel and propylamine as template was successful, the n_{Si}/n_{Al} ratio of the product was 14, which is the same as for the product B1. This finding indicates that the minimum n_{Si}/n_{Al} ratio of aluminum-containing products is 14. The synthesis experiments with n_{Si}/n_{Al} = 3 in the synthesis gel using propylamine as template did not yield crystalline products.

As mentioned above, the powder XRD patterns of the aluminum-containing ferrierite zeolites show pure FER phases (see Figure 1b). Furthermore, it was confirmed by ^{27}Al MAS NMR spectroscopy that the aluminum was incorporated into the framework of the ferrierite zeolites. Figures 5a to 5c show the ^{27}Al MAS NMR spectra of as-synthesized large-crystal aluminum-containing ferrierite zeolites prepared using different alkylamines as templates and pyridine as solvent. These spectra are dominated by a signal at about 53 ppm, which is due to tetrahedrally coordinated framework aluminum species. In the ^{27}Al MAS NMR spectrum of the sample obtained via batch B2 (Figure 5b), a very weak signal at about 0 ppm due to octahedrally coordinated nonframework aluminum species was observed. Figure 5d represents the ^{27}Al MAS NMR spectrum of the calcined and rehydrated form of aluminum-containing ferrierite zeolite synthesized using pentylamine as template and pyridine as solvent. The spectrum shows only a single peak at about 54 ppm corresponding to tetrahedrally coordinated framework aluminum species. This finding indicates that the aluminum remains in the framework even after calcining the sample under a flow of synthetic air at 873 K for 4 days.

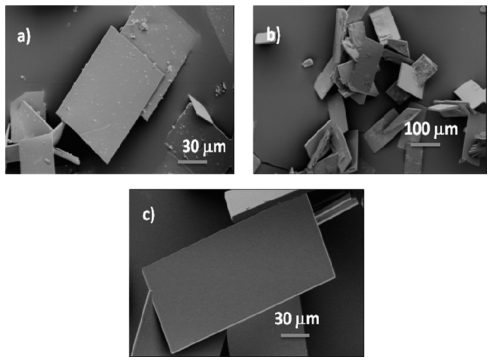

Figure 6. SEM images of the large-crystal aluminum-containing ferrierite zeolites synthesized using propylamine (a), sample B1, butylamine (b), sample B2, and pentylamine (c), sample B3, as templates with n_{Si}/n_{Al} = 6 in the synthesis gel.

Figure 6 shows the SEM images of aluminum-containing ferrierite zeolites synthesized using different alkylamines as templates and pyridine as solvent in the synthesis (batches B1 to B3). In contrast to all-silica ferrierite zeolites (Figure 4), the morphologies of the three aluminum-containing ferrierite zeolites are similar, irrespective of the template employed in the synthesis (Figure 6). Nevertheless, slightly larger crystallites were obtained when increasing the length of the alkyl chain in the template molecule and the crystallization time. With the use of propylamine, butylamine, and pentylamine as templates and pyridine as solvent in the synthesis, the crystal sizes of the aluminum-containing ferrierite samples were about 100, 150, and 180 μm, respectively. The crystal sizes of the samples obtained in the present work were slightly smaller than those of the samples obtained by Ozin and co-workers.[9,11]

Even though the isomorphous substitution of boron into the framework of MFI-, MEL-, Beta-, and RUT-type zeolites was successful, literature concerning the synthesis of boron-containing ferrierite zeolite is very scarce.[17,18,32−34] Gies and co-workers[17,18] attempted to synthesize aluminum-free ferrierite zeolite using the ethylenediamine-boric acid complex as template. They obtained aluminum-free ferrierite, but the boron incorporation into the FER framework was unsuccessful. Moreover, their synthesis method furnished a mixture of a FER and an MFI phase. Perego et al.[33,34] also tried to synthesize boron-containing ferrierite ([B]FER) using an aqueous solution of tetramethoxysilane, boric acid, and ethylenediamine. However, this synthesis method led to the crystallization of boron-containing MFI-type zeolites accompanied by small amounts of [B]FER. To the best of our knowledge, our solvothermal synthesis method in a fluoride medium is the first successful approach leading to boron-containing ferrierite zeolites with a pure FER framework (except sample C3).

In the present work, boron-containing ferrierite samples were synthesized using n_{Si}/n_B = 3 to 6 in the synthesis gel (batches C1 to C6). However, the n_{Si}/n_B ratios of the products were in the range of 35 to 325 (see Table 1). This finding indicates that a large amount of boron atoms remained in the mother liquor. This behavior was generally expected for the synthesis of boron-containing zeolites.[32−34] Even when the n_{Si}/n_B ratio in the synthesis gel was kept constant, as-synthesized products with

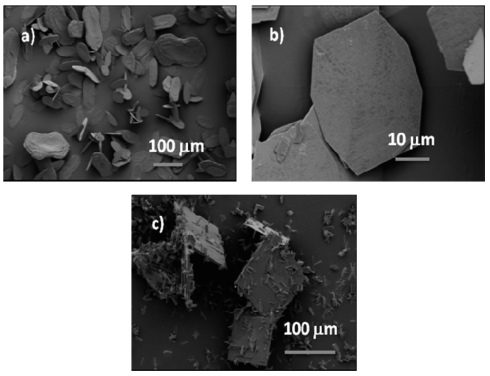

Figure 7. SEM images of the large-crystal boron-containing ferrierite zeolites synthesized using propylamine (a), sample C1, butylamine (b), sample C2, and pentylamine (c), sample C3, as templates with $n_{Si}/n_B = 3$ in the synthesis gel.

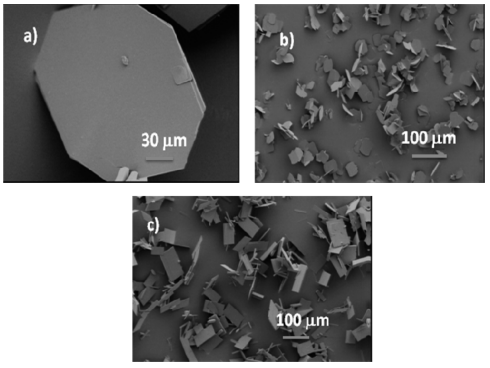

Figure 8. SEM images of the large-crystal boron-containing ferrierite zeolites synthesized using propylamine (a), sample C4, butylamine (b), sample C5, and pentylamine (c), sample C6, as templates with $n_{Si}/n_B = 6$ in the synthesis gel.

significantly different n_{Si}/n_B ratios were obtained (see Table 1, batches C1 to C6). This could be due to the different templates (e.g., propylamine, butylamine, and pentylamine) and crystallization times of the syntheses. As a result, products with different crystal sizes and shapes were obtained. Figures 7 and 8 show the SEM images of the boron-containing ferrierite samples synthesized using different templates and with n_{Si}/n_B = 3 and 6 in the gel. With n_{Si}/n_B = 3 in the synthesis gel, using propylamine, butylamine, as well as pentylamine as templates and pyridine as solvent, stretched hexagonal/octagonal shapes with rough surfaces (Figure 7a), octagonal (Figure 7b), and a combination of small stretched hexagonal and large square plates (Figure 7c), respectively, were obtained. For sample C3 (Figure 7c), two types of crystals were observed because of the presence of FER and MFI phases. Upon doubling the n_{Si}/n_B ratio in the synthesis gel to 6, the SEM pictures showed large crystals with octagonal morphologies with smooth surfaces when using propylamine and butylamine as templates (Figures 8a and 8b). In contrast, large, rectangular, and flat crystals (Figure 8c) with smooth surfaces were obtained when using pentylamine as template (batch C6) and pyridine as solvent.

To verify the boron incorporation into the framework of ferrierite zeolite, ^{11}B MAS NMR spectroscopy was utilized in this work. As shown in Figures 9a to 9c, the ^{11}B MAS NMR spectra of the as-synthesized boron-containing ferrierite zeolites synthesized using different alkylamines as templates and pyridine as solvent

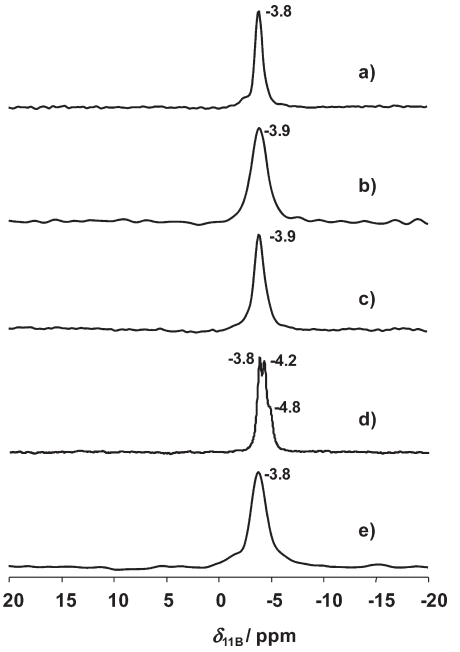

Figure 9. ^{11}B MAS NMR spectra of as-synthesized large-crystal boron-containing ferrierite zeolites prepared using propylamine (a), sample C4, butylamine (b), sample C5, and pentylamine (c), sample C6, as templates. In (d), the spectrum of the calcined and dehydrated sample of (b) and in (e) the spectrum of the calcined and rehydrated sample of (b) are shown.

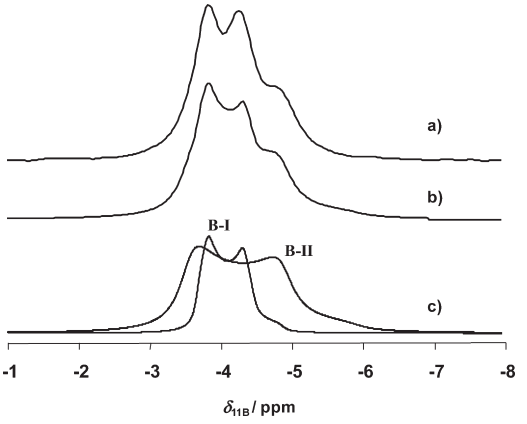

Figure 10. ^{11}B MAS NMR spectra of calcined and dehydrated boron-containing ferrierite zeolite, sample C5. Experimental (a), simulated (b), and components (c) of the spectra are presented.

exhibit a single narrow signal at −3.8 ppm to −3.9 ppm with a quadrupole coupling constant of C_{QCC} = 0.8 MHz. This signal was attributed to tetrahedrally coordinated framework boron atoms in boron-containing ferrierite zeolites.[35]

The ^{11}B MAS NMR spectrum (Figures 9d) of the calcined and dehydrated boron-containing ferrierite zeolite (i.e., sample C5) shows three peaks at −3.8 ppm, −4.2 ppm, and −4.8 ppm. The peaks are clearly visible in Figure 10, where also their simulation is presented. Simulation was performed using two components of framework boron species (i.e., B−I and B−II). From the simulation, quadrupole coupling constants of C_{QCC} = 0.6 MHz and C_{QCC} = 0.8 MHz were obtained for B−I and B−II species, respectively. As already shown in the ^{29}Si MAS NMR spectra

dx.doi.org/10.1021/cm1014898 |*Chem. Mater.* 2011, 23, 2521–2528

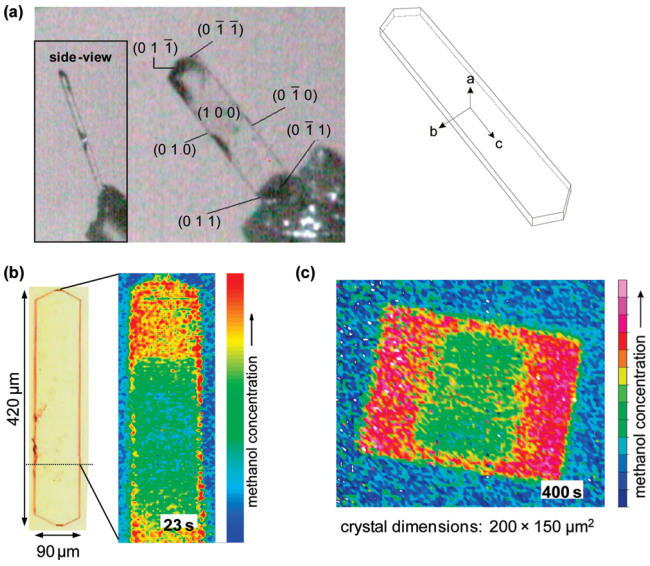

Figure 11. Crystallographic orientation of the largest faces of an all-silica ferrierite crystal from sample A2 as determined by single-crystal X-ray analysis (a). Images recorded by IR microscopy at 298 K (b, c). Snapshot of the methanol distribution in an all-silica ferrierite crystal (i.e., sample A2), 23 s after starting the uptake. The crystal size exceeds that of the detector and is cut at the lower end (b). Uptake profile in an aluminum-containing ferrierite crystal (see sample B1 in Table 1 and Figure 6a) 400 s after a step change in the surrounding gas phase (c). The different channel diameters of the two pore systems give rise to a pronounced anisotropy in their uptake rates. The uptake in the all-silica sample is faster by a factor of about 20.

(Figure 3), there exist different nonequivalent T-sites in the asymmetric unit of space group *Pmnn*.[2,30,31] Hence, the occurrence of two kinds of B−I and B−II signals in the present case could be due to boron incorporated at different crystallographic positions in the crystal structure. In comparison with the quadrupolar patterns of trigonal framework boron described in the literature,[35−37] very narrow quadrupole patterns were obtained for framework boron species B−I and B−II indicating a higher symmetry of their local structure like for tetrahedrally coordinated framework boron species. Upon rehydration of the sample C5 for at least 12 h, the reoccurrence of the ^{11}B MAS NMR signal (Figure 9e) at −3.8 ppm indicates the stable incorporation of boron into the framework of the large-crystal boron-containing ferrierite. Moreover, the signal corresponding to nonframework trigonal boron species, which generally appears at higher fields (ca. 18 ppm), was not observed in the present samples.[36,37]

The accessibility of the channel network from the outer surface was examined by monitoring transient intracrystalline guest profiles using interference microscopy (IFM) and IR microscopy (IRM) with methanol as a guest molecule. As discussed in the beginning, in the all-silica ferrierite samples of a first series of syntheses[12] the entrances of the 10-membered-ring channels were found to be blocked.[5,6] Initially, also in the all-silica ferrierite sample synthesized and investigated in this work, no methanol uptake along the 10-membered-ring channels was detected, indicating a strong external surface resistance.

In the synthesis of MFI-type crystals, postsynthesis washing of the crystallites in NaOH solution is routinely applied to remove potentially existing amorphous residues from the solids.[38] This procedure turned out to be particularly useful to open the 10-membered ring channels for methanol uptake and was, thus, included in all our syntheses (see Section 2.3). In samples A2, A3, B1, and B3 either no or only very weak surface resistances were found. Surface etching with HF solutions could provide a further option to reduce or eliminate outer surface resistances.[39,40]

To set the background for the interpretation of our diffusion data and to check the crystals for twinning, the crystallographic orientation of the largest faces was determined in single-crystal X-ray studies. In all cases the direction [0 0 1] of the 10-membered ring channels was found to coincide with the longest extension of the crystallites, whereas the direction [0 1 0] of 8-ring channels was found to run along the second longest crystal side. Hence, the channel network is always extended in the large crystal plane, no channels are running in the [1 0 0] direction. For illustration, the indexing of one crystal from batch A2 is shown in Figure 11a.

Our previous studies[5,6] suggested a pronounced diffusion anisotropy of methanol in the channel network of all-silica ferrierite. The blockage of the entrances to the 10-membered ring channels prohibited a direct evidence of this phenomenon. Now, diffusion anisotropy of methanol could be confirmed and quantified in both the all-silica sample A2 and the aluminum-containing ferrierite sample B1. Depending on the loading, diffusivities range from 10^{-10} to 10^{-9} m^2 s^{-1} along the larger 10-ring channels and from 10^{-13} to 10^{-11} m^2 s^{-1} along the smaller 8-ring channels, resulting in a diffusion anisotropy of 2 to 3 orders of magnitude in the all-silica sample A2. Surprisingly, the anisotropy in sample B1 (aluminum-containing ferrierite) is reduced by a factor of 10−20. This is caused by a corresponding pronounced reduction of the methanol diffusivity along the 10-ring channels, while the mobility along the 8-ring channels remains nearly unaffected.

The anisotropy is illustrated in Figures 11b and 11c where snapshots of the methanol distribution in crystallites of, respectively, the all-silica sample (A2) and of the aluminum-containing ferrierite (sample B1 of Table 1) are shown.[6] The relative concentration of the methanol molecules was obtained from the intensity of characteristic IR absorption bands and visualized by color contrast in the plot. Figure 11b was recorded already 23 s after a step change in the surrounding atmosphere of the all-silica sample. Nevertheless, the concentration front has already proceeded somewhat further into the crystal than in the case of the aluminum-containing ferrierite sample (Figure 11c), which was recorded 400 s after starting the uptake, indicating a much higher diffusivity along the 10-ring channels of the all-silica sample. The loading step was comparable in both cases.

To study the impact of metal-ion incorporation in the framework on the molecular transport and for further characterization of the diffusion properties, systematic diffusion studies of different guest molecules are currently in our focus and will be discussed in a following publication.

4. CONCLUSIONS

The aim of the present study was to systematically investigate the solvothermal synthesis of large-crystal all-silica, aluminum-, and boron-containing ferrierite zeolites using different alkylamines as templates and pyridine as solvent. In the case of all-silica and boron-containing ferrierite zeolites, the use of different templates and crystallization times led to the formation of large crystals with sizes of up to 600 μm and up to 150 μm, respectively, and hexagonal/octagonal, stretched hexagonal,

and rectangular flat morphologies. In contrast, for aluminum-containing ferrierite zeolites, rectangular flat crystals with sizes of up to 180 μm were obtained irrespective of the alkylamine used in the synthesis. Furthermore, the synthesis of aluminum-containing and boron-containing ferrierite zeolites was carried out using relatively high aluminum and boron contents (i.e., n_{Si}/n_{Al} = 4.5 to 6 and n_{Si}/n_B = 3 to 6) in the synthesis gel. ^{27}Al and ^{11}B MAS NMR spectroscopic investigations revealed the successful incorporation of aluminum and boron into the FER-type structure. The thus synthesized FER-type crystals permit the direct measurement of diffusion anisotropy. They were in particular found to permit the accessibility of both channel types from the external surface. The in-depth study of molecular diffusion in these materials is in the focus of our ongoing work.

AUTHOR INFORMATION

Corresponding Author

*Phone: +49 711 685 64060. Fax: +49 711 685 64065. E-mail: jens.weitkamp@itc.uni-stuttgart.de.

ACKNOWLEDGMENT

The authors gratefully acknowledge financial support by the German Science Foundation (DFG).

REFERENCES

(1) Barrer, R. M. *J. Chem. Soc.* **1948**, 127.
(2) Weigel, S. J.; Gabriel, J.-C.; Puebla, E. G.; Bravo, A. M.; Henson, N. J.; Bull, L. M.; Cheetham, A. K. *J. Am. Chem. Soc.* **1996**, *118*, 2427.
(3) Scandella, L.; Binder, G.; Mezzacasa, T.; Gobrecht, J.; Berger, R.; Lang, H. P.; Gerber, Ch.; Gimzewski, J. K.; Koegler, J. H.; Jansen, J. C. *Microporous Mesoporous Mater.* **1998**, *21*, 403.
(4) Di Renzo, F. *Catal. Today* **1998**, *41*, 37.
(5) Kärger, J.; Kortunov, P.; Vasenkov, S.; Heinke, L.; Shah, D. B.; Rakoczy, R. A.; Traa, Y.; Weitkamp, J. *Angew. Chem., Int. Ed.* **2006**, *45*, 7846.
(6) Heinke, L.; Chmelik, C.; Kortunov, P.; Ruthven, D. M.; Shah, D. B.; Vasenkov, S.; Kärger, J. *Chem. Eng. Technol.* **2007**, *30*, 995.
(7) Shimizu, S.; Hamada, H. *Angew. Chem., Int. Ed.* **1999**, *38*, 2725.
(8) Lethbridge, Z. A. D.; Williams, J. J.; Walton, R. I.; Evans, K. E.; Smith, C. W. *Microporous Mesoporous Mater.* **2005**, *79*, 339.
(9) Kuperman, A.; Nadimi, S.; Oliver, S.; Ozin, G. A.; Garcés, J. M.; Olken, M. M. *Nature* **1993**, *365*, 239.
(10) Morris, R. E.; Weigel, S. J. *Chem. Soc. Rev.* **1997**, *26*, 309.
(11) Nadimi, S.; Oliver, S.; Kuperman, A.; Lough, A.; Ozin, G. A.; Garcés, J. M.; Olken, M. M.; Rudolf, P. In *Zeolites and Related Microporous Materials: State of the Art 1994, Studies in Surface Science and Catalysis*; Weitkamp, J., Karge, H. G., Pfeifer, H., Hölderich, W., Eds.; Elsevier: Amsterdam, The Netherlands, 1994; Vol. 84, Part A, p 93.
(12) Rakoczy, R. A.; Traa, Y.; Kortunov, P.; Vasenkov, S.; Kärger, J.; Weitkamp, J. *Microporous Mesoporous Mater.* **2007**, *104*, 179.
(13) http://www.iza-structure.org/databases/.
(14) Wise, W. S.; Tschernich, R. W. *Am. Mineral.* **1976**, *61*, 60.
(15) Barrer, R. M.; Marshall, D. J. *J. Chem. Soc.* **1964**, 485.
(16) Barrer, R. M.; Marshall, D. J. *Am. Mineral.* **1965**, *50*, 484.
(17) Gies, H.; Gunawardane, R. P. *Zeolites* **1987**, *7*, 442.
(18) Gunawardane, R. P.; Gies, H.; Marler, B. *Zeolites* **1988**, *8*, 127.
(19) Forbes, N. R.; Rees, L. V. C. *Zeolites* **1995**, *15*, 444.
(20) Schreyeck, L.; Caullet, P.; Mougenel, J.-C.; Guth, J.-L.; Marler, B. *J. Chem. Soc., Chem. Commun.* **1995**, 2187.
(21) Guo, G.-q.; Sun, Y.-j.; Lai, Y.-c. *Chem. Commun.* **2000**, 1893.
(22) Wirnsberger, G.; Fritzer, H. P.; Koller, H.; Behrens, P.; Popitsch, A. *J. Mol. Struct.* **1999**, *480−481*, 699.
(23) Rakoczy, R. A.; Breuninger, M.; Hunger, M.; Traa, Y.; Weitkamp, J. *Chem. Eng. Technol.* **2002**, *25*, 273.
(24) Sulikowski, B.; Klinowski, J. *J. Chem. Soc., Chem. Commun.* **1989**, 1289.
(25) Borade, R. B.; Clearfield, A. *Chem. Commun.* **1996**, 2267.
(26) Ahedi, R. K.; Kotasthane, A. N. *J. Mater. Chem.* **1998**, *8*, 1685.
(27) Shevade, S. S.; Rao, B. S. *J. Mater. Chem.* **1999**, *9*, 2459.
(28) Davidson, A.; Weigel, S. J.; Bull, L. M.; Cheetham, A. K. *J. Phys. Chem. B* **1997**, *101*, 3065.
(29) Darton, R. J.; Morris, R. E. *Solid State Sci.* **2006**, *8*, 342.
(30) Morris, R. E.; Weigel, S. J.; Henson, N. J.; Bull, L. M.; Janicke, M. T.; Chmelka, B. F.; Cheetham, A. K. *J. Am. Chem. Soc.* **1994**, *116*, 11849.
(31) Bull, L. M.; Bussemer, B.; Anupõld, T.; Reinhold, A.; Samoson, A.; Sauer, J.; Cheetham, A. K.; Dupree, R. *J. Am. Chem. Soc.* **2000**, *122*, 4948.
(32) Millini, R.; Perego, G.; Bellussi, G. *Top. Catal.* **1999**, *9*, 13.
(33) Perego, G.; Bellussi, G.; Millini, R.; Alberti, A.; Zanardi, S. *Microporous Mesoporous Mater.* **2002**, *56*, 193.
(34) Perego, G.; Bellussi, G.; Millini, R.; Alberti, A.; Zanardi, S. *Microporous Mesoporous Mater.* **2003**, *58*, 213.
(35) Marthala, V. R. R.; Wang, W.; Jiao, J.; Jiang, Y.; Huang, J.; Hunger, M. *Microporous Mesoporous Mater.* **2007**, *99*, 91.
(36) Hwang, S.-J.; Chen, C.-Y.; Zones, S. I. *J. Phys. Chem. B* **2004**, *108*, 18535.
(37) Fild, C.; Shantz, D. F.; Lobo, R. F.; Koller, H. *Phys. Chem. Chem. Phys.* **2000**, *2*, 3091.
(38) Schmidt, W.; Wilczok, U.; Weidenthaler, C.; Medenbach, O.; Goddard, R.; Buth, G.; Cepak, A. *J. Phys. Chem. B* **2007**, *111*, 13538.
(39) Wloch, J. *Microporous Mesoporous Mater.* **2003**, *62*, 81.
(40) Brabec, L.; Kocirik, M. J. *Phys. Chem. C* **2010**, *114*, 13685.